POLITECNICO
MILANO 1863

SCUOLA DI INGEGNERIA INDUSTRIALE
E DELL'INFORMAZIONE

Executive Summary of the Thesis

Synthesis and Characterization of Manganese Oxides Thin Films

Laurea Magistrale in Materials and Nanotechnology Engineering - Ingegneria dei Materiali e delle Nanotecnologie

Author: Arianna Monforte Ferrario

Advisor: Prof. Andrea Li Bassi

Co-advisor: Dr. Andrea Macrelli

Academic year: 2021-2022

1. Introduction

Manganese oxides (MnO_x) are naturally abundant, low cost and environmental friendly materials that have been used for thousands of years for various applications in different fields ranging from art to steelmaking and environmental safety. Recently, they have become very attractive for their potential application in electrical energy storage and conversion devices such as electrochemical capacitors and supercapacitors, electrocatalysts, and various types of batteries but, however, they present some critical aspects to be addressed. Indeed, the multiple oxidation states of manganese (+2, +3, +4, +6, and +7) give rise to a plethora of different phases which are often hard to be caracterized by standard methods. Moreover, such complexity is reflected in the electrochemical behavior of these materials which involves numerous complex phase transitions and ranges over different oxidation states of manganese. In this context, the synthesis of pure phases of MnO_x can play a fundamental role both in shedding light on the controversial situation concerning the assignment of the different MnO_x phases, and in the study of the complex electrochemical behavior of these materials.

2. Manganese Oxides materials

More than 30 manganese (Mn) oxide/hydroxide minerals can be found in a variety of geological systems and are nearly ubiquitous in soils and sediments. Most Mn oxide minerals are brown-black and typically occur as fine-grained mixtures of different Mn phases plus additional minerals such as carbonates, silicates, and iron oxides/hydroxides. Although MnO_x exist with a continuous range of compositions between MnO and MnO_2, it is MnO_2 which is by far the most important oxide of the group. The basic building block for most MnO_x atomic structures (expecially MnO_2) is the MnO_6 octahedron which can give rise to a large variety of different tunnel or layer structures by sharing edges and/or corners. Among the various morphologies and crystallographic forms of manganese dioxide (MnO_2), the $\alpha-$, $\beta-$, $\gamma-$, $R-$, and $T-$ polymorphs are characterized by different tunnel structures, while only the $\delta-MnO_2$ phase exhibits a layer structure. Other forms of MnO_2 are the $\epsilon-$ and $\lambda-$ polymorphs which show a dense packed structure and a three-dimensional spinel structure respectively [1]. Despite the MnO_2 phase is the most abundant, other MnO_x such as the Mn_3O_4, Mn_2O_3 and

MnO also exist. The first two phases are usually obtained at high temperatures and have a tetragonally-distorted spinel structure and a cubic structure respectively; while the MnO phase exhibits a rock-salt structure and it is obtained by reduction with hydrogen of any other oxide of manganese.

The poor crystallinity of MnO_x, the size of the crystallites typically limited to the nanoscale, and the presence of multiple associated phases make the identification and proper characterization of natural MnO_x a real challenge by standard methods such as as X-ray powder diffraction (XRPD). Spectroscopic techniques provide a valuable tool for studying these minerals, being sensitive to short-range metal-oxygen arrangements. In particular, Raman Spectroscopy is a valuable complementary technique for the investigation of these materials, being a fast, non-destructive method that can provide information about local atomic coordination environments as well as longer-range structure, and therefore can be a useful identification technique even for highly disordered materials. However, even though this technique was widely used for the recognition of MnO_x, reliable literature reference data are missing due to strong discrepancies between the different authors. These disagreements can be due to many factors such as the experimental condition, the incorrect identification of the examined cryptocrystalline materials, and the wide variety of possible mixtures between different MnO_x. Moreover, MnO_x have a low Raman activity and are very sensitive to the laser heating. In fact, the strong absorption of photon energy by the blackish MnO_x produces a local heating that can cause shifts and broadening of the Raman peaks due to photo-induced or thermal-induced chemical reactions. This issue is complicated by the effects of different laser wavelengths, power densities, and optics used for data collection. Lastly, some MnO_x have characteristic Raman spectra and can be easily recognized by using Raman spectroscopy alone, but in order to characterize different MnO_x phases that show nearly identical Raman spectra, integration of Raman data with other techniques is mandatory.

Manganese oxides have been widely used in a wide range of applications over the millenia, from art works, to steelmaking and as important geomaterials for environmental applications. However, the current growing demand for energy in a world increasingly ravaged by climate change, has greatly increased interest in renewable energy resources and, conseguently, on reliable, high-performance and safe electrical energy storage (EES) devices. Therefore, extensively used in industry for more than a century, MnO_x now find great renewal of interest as nanostructured materials with very attractive physicochemical properties for storage and conversion of energy applications. In particular, the excellent electrochemical properties of several MnO_x phases are attracting much attention for positive electrode materials for Lithium- (Li) and Zinc- (Zn) ion-batteries and for catalytic and photocatalytic applications. This generates an important activity in the field of Solid State Chemistry to synthesise new phases of MnO_x with optimized nanostructure and improved electrochemical properties.

The objectives of this thesis may be summarized in the following points:

1. Synthesis of pure MnO_x phases in the form of thin films by Pulsed Laser Deposition [2] at room temperature in oxygen atmosphere and subsequent thermal treatments, to obtain a decoupled control of the phase and nanoscale morphology/porosity of the films;
2. Characterization of the produced films by different techniques and the correlation of the material properties to the parameters used for the synthesis. In particular, the characterization of the films by Raman Spectroscopy and X-Ray Diffraction may help to better clarify the controversial situation surrounding the assignment of different MnO_x phases;
3. Prelyminary electrochemical tests on thin films as model systems to provide the foundation for future studies aimed at clarifying the electrochemical behavior of these materials in aqueous electrolyte.

3. Synthesis and characterization of as-deposited MnO_x films

In this work, Pulsed Laser Deposition (PLD) [2] at room temperature was used to produce thin films of MnO_x. Films with desired thickness and uniformity were obtained by varying the background O_2 pressure and the target-substrate misalignment. The films were deposited by ablating a MnO target at different O_2 partial pressures (i.e., 1 Pa, 10 Pa, 50 Pa, 100 Pa) on silicon substrate, by keeping constant the laser parameters (i.e., 532 nm wavelength, ~ 2 J/cm^2 fluence) and the target-to-substrate distance (5 cm).

The effect of the deposition O_2 pressure on the morphology of the films was analysed through Scanning Electron Microscopy (SEM). The SEM images revealed that as the deposition O_2 pressure increases, the morphology of the deposited film becomes less and less compact, and progressively develop a "tree-like structure" with increased nanoporosity and, consequently, effective surface area (Figure 1).
Phase characterization of as-deposited films was performed by means of Raman Spectroscopy, Energy Dispersive X-Ray Spectroscopy (EDX), and X-Ray Diffraction. Given the well-known problems related to the stability of these materials under the laser beam, a detailed investigation of the effect of laser power and wavelength on the MnO_x films was conducted and the green laser 532 nm resulted to be the best choice for the characterization of the films. The Raman spectra of the as-deposited films (Figure 2) revealed that the O_2 pressure also has influence on the resulting MnO_x phase. All samples, except the one deposited at 1 Pa of O_2, show a Raman spectrum characterized by a broad band centered at about 600−650 cm^{-1}, and extending between 400 and 800 cm^{-1}, typical of amorphous manganese oxides. Indeed, by performing a Lorentzian fitting, I found that this band is actually structured in three peaks at $\sim$ 501−502 cm^{-1}, $\sim$ 564−575 cm^{-1}, and $\sim$ 537−538 cm^{-1} typical of the $\delta-MnO_2$ phase according to [3]. On the other hand, the Raman spectrum of the sample deposited at 1 Pa exhibits three well defined peaks at $\sim$ 323 cm^{-1}, $\sim$ 378 cm^{-1}, and $\sim$ 665 cm^{-1} which are index of a crystalline phase and close to the peaks of Mn_3O_4 [3].

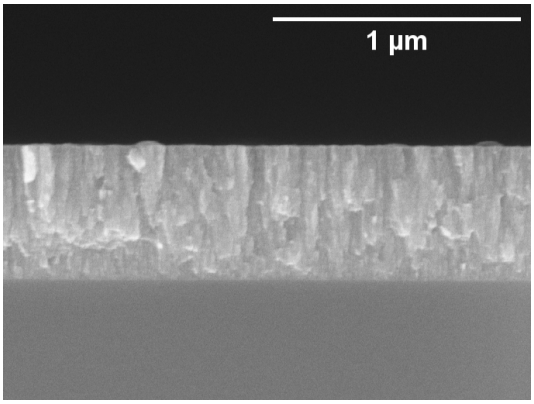

(a)

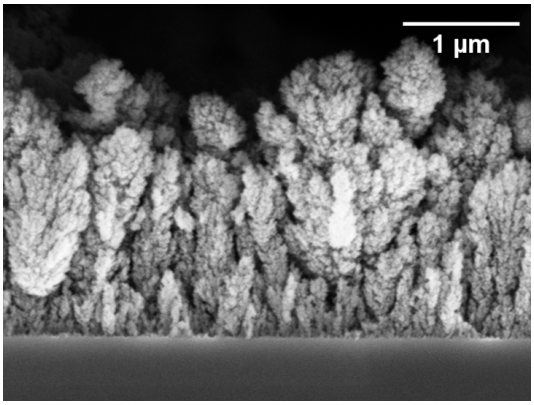

(b)

Figure 1: SEM images of as-deposited MnO_x films produced at 10 and 100 Pa of oxygen, respectively.

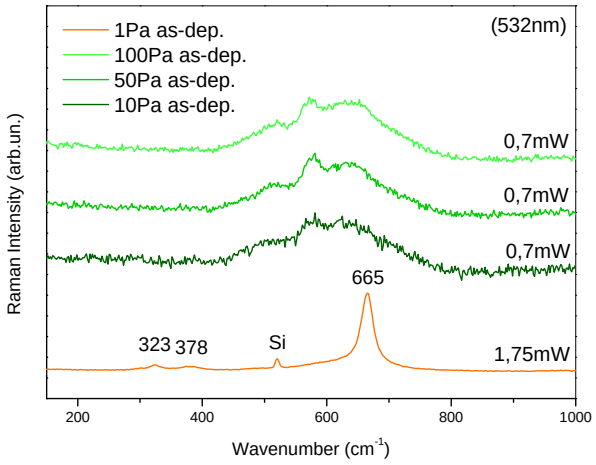

Figure 2: Raman spectra of MnO_x films deposited at 1 Pa, 10 Pa, 50 Pa, and 100 Pa of oxygen on silicon substrate.

These results are also confirmed by EDX (which provides Mn/O ratios compatible with the assigned phases, here not shown) and XRD analysis. In particular, XRD measurements (not shown), conducted on selected samples (i.e., 1 Pa and 10 Pa), added further information about the crystallinity of the films. The sample deposited at 10 Pa shows a very noisy XRD pattern and no defined peaks are visible except for a wide peak around 17°. The sample deposited at 1 Pa, instead, shows three main broad and asymmetric peaks that could be assigned to the (101), (112) and (103) reflections of the Mn_3O_4 phase. However, also in this case the signal-to-noise ratio of the XRD pattern is poor and not all peaks related to the Mn_3O_4 phase are present. The bad quality of XRD patterns could be index of low crystalline quality (i.e., poorly crystallized or amorphous material) or of very small crystals. Furthermore, since, unlike Raman, XRD is sensitive to the long range order, the combination of these two techniques can be used to have an idea on how well the material is globally ordered. Therefore, considering the results of Raman, EDX, and XRD analysis, I can state that via PLD depositions in O_2 atmosphere, I obtained two different MnO_x phases: nanocrystalline Mn_3O_4 and some form of amorphous MnO_2. In particular, I am confident to think that what I obtained from the deposition at 1 Pa of O_2 is actually a nanocrystalline Mn_3O_4 phase dispersed in an amorphous matrix.

Lastly, depositions on glass substrate were also performed with the aim of studying also the optical properties of as-deposited films. The optical transmittance, reflectance and absorbance of as-deposited MnO_x films (here not shown) were measured, and a fundamental optical characterization was accomplished.

4. Characterization of annealed MnO_x films

The introduction of post-deposition heat treatments was driven by the following idea: being able to decouple, as far as possible, the phase, crystallinity and morphology control by combining different deposition pressures and annealing treatments. In particular, the choice of the annealing temperature and atmosphere was discovered to be a key parameter to obtain different MnO_x phases. The MnO_x films were annealed in air at temperatures of 300°C for 4 h, at 500°C and 900°C for 2 hours, and in vacuum at 500°C for 1 hour.

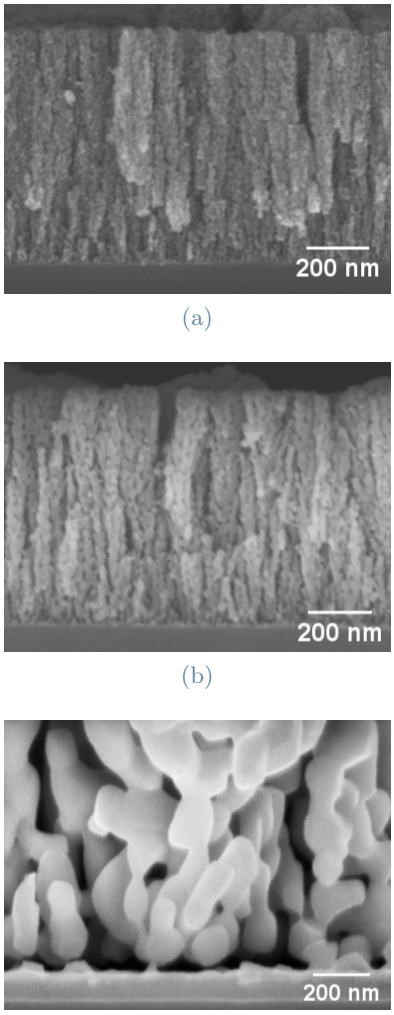

(a) (b) (c)

Figure 3: SEM images of MnO_x films deposited at 50 Pa and annealed in air at 300°C (a), 500°C (b) and 900°C (c).

Regarding the annealing in air, the SEM analysis (Figure 3) reveals initial formation of nanosized grains since the thermal treatment conducted at 300°C, and a further progressive increase in the grains size and crystalline quality by increasing the annealing temperature. In particular, at very high temperatures (i.e., 900°C) I observe a strong sintering effect and coalescence of the grains. On the other hand, annealing in vacuum (whose SEM images are here not shown), compared with the thermal treatment

conducted in air at the same temperature (i.e., 500°C), leads to the formation of coarse grains and a more disordered overall structure (mainly visible in samples deposited at 1 and 10 Pa).

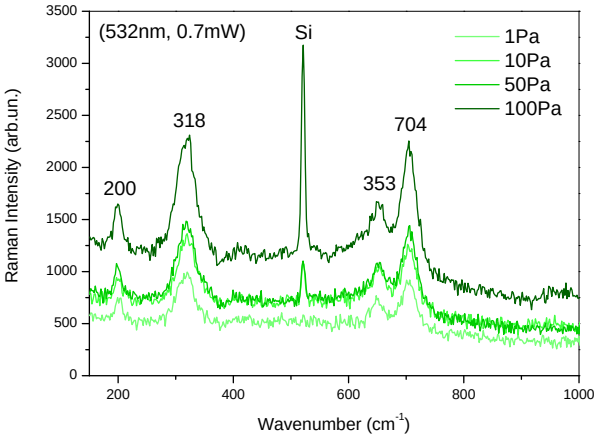

Figure 4: Raman spectra of air-annealed MnO_x films deposited at 1 Pa, 10 Pa, 50 Pa, and 100 Pa of oxygen on silicon substrate.

While the annealing temperature has a strong impact on the morphology of the films, the annealing atmosphere was discovered to have more influence in determining the MnO_x phase. In fact, Raman analysis conducted on annealed films shows that from different annealing atmospheres two MnO_x phases can be obtained. The Raman spectra for the samples annealed in air (Figure 4) exhibit four main peaks at $\sim$ 200 cm^{-1}, $\sim$ 318 cm^{-1}, $\sim$ 353 cm^{-1}, and $\sim$ 704 cm^{-1} which are fingerprint of the Mn_2O_3 phase according to [3]. However, the Mn_2O_3 phase was found to appear only for temperatures $\geq$ 500°C while for lower temperatures, the amorphous-like MnO_x phase coming from the PLD deposition is preserved. As regards the annealing in vacuum, Raman analysis revealed that the Mn_3O_4 phase was obtained. However, comparing the Raman spectra of samples annealed in vacuum (here not shown) and of the sample as-deposited at 1 Pa of O_2, I noted that the ones related to the annealed samples exibit a better definiton of the peaks, with reduced FWHM and a better signal-to-noise ratio. This further confirms the hypothesis according to which the PLD at room temperature at 1 Pa produces a dispersion of nanocrystals of Mn_3O_4 in an amorphous matrix while the thermal treatment in vacuum leads to the formation of a single Mn_3O_4 nanocrystalline phase. Also in this case EDX and XRD measurements were performed in order to confirm the results obtained. In particular, the well defined XRD patterns (Figure 5) provide overwhelming proof of the correct assignment of the MnO_x phases obtained.

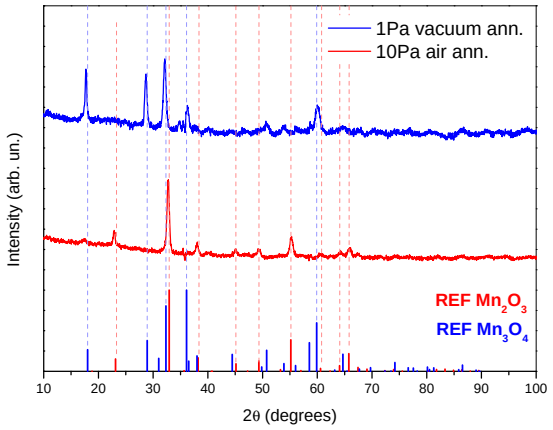

Figure 5: XRD patterns of annealed MnO_x films at 1 Pa (in vacuum) and 10 Pa (in air) O_2 pressure compared with the reference.

With the aim to perform optical characterization also on the annealed MnO_x films, thermal treatments were performed on films deposited on glass substrate. However, I discovered that the substrate can have an influence on the resulting MnO_x phase obtained and such effect is activated by temperature. Raman and XRD analysis conducted on the film deposited on glass at 10 Pa of O_2 and annealed in air at 500°C revealed the occurrence of a new MnO_2 phase different from the one directly obtained by PLD and from the Mn_2O_3 phase resulting from air-annealing on silicon substrate: the $\alpha-MnO_2$ phase, probably stabilized by cations provided by the glass. Since more extensive experiments are needed to completely understand the effect of the glass substrate on the resulting MnO_x phase, optical properties on annealed films are not reported in this study.

5. Early electrochemical tests on MnO_x films

This section presents the preliminary investigation of the electrochemical behaviour of MnO_x films performed by means of Ciclic Voltammetry (CV) conducted on selected MnO_x samples. The

three-electrode configuration used consists in a Teflon cell, two platinum wires as counter and quasi-reference electrodes, and the MnO_x film as working electrode. The CV tests were conducted in two different electrolytes ($\sim$ 1 mL): Na_2SO_4 0.2 M (NS electrolyte) and $ZnSO_4$ 2 M + $MnSO_4$ 0.1 M (ZMS electrolyte). Since the electrochemical behaviour of MnO_x materials is rather complex (involving complicated phase transitions, intermediate compounds, and multiple oxidation states) and depends on many experimental parameters (MnO_x phase, electrolyte composition and pH) [4], the NS electrolyte was chosen due to its inertness in the investigated potential ranges (see below) to study the fundamental electrochemical behaviour of the film itself; while the ZMS electrolyte was used to simulate a more realistic situation of a zinc battery.
The films used for the electrochemical tests were produced by PLD at different oxygen pressures (1 Pa, 10 Pa, and 50 Pa) on FTO-coated glass substrates. Both as-deposited samples, annealed in air at 500°C for 2 h, and annealed in vacuum at 500°C for 1 h were tested. Deposition time at any O_2 pressure was set in order to obtain a film thickness of $\sim$ 500 nm.

First electrochemical tests were performed with the NS electrolyte. The CV was performed with the potential scanning in a range of -1.45 V to +1.05 V vs. Pt-QRef., starting at 0 V, proceeding in anodic direction, and adopting a scan rate of 10 mV/s for ten cycles.
From the CVs of as-deposited films (not shown), a correlation between the O_2 deposition pressure and the amount of charge exchanged during the electrochemical process can be observed. This fact, highlighted by the incresing of the area of the CVs by increasing the deposition pressure, is reasonable in view of the fact that films deposited at higher O_2 pressures are more porous and therefore exhibit a greater surface area for electrochemical reactions. By Raman and SEM analysis I was able to confirm that independently of the starting MnO_x phase and morphology of the films, the electrochemical process leads to the formation of *electrodeposited manganese oxide* (EDM), which is a mix of MnO_x in which some forms of MnO_2 (e.g., δ-, γ-, [4] etc.) are mainly present. This is confirmed both by the fibrous morphology of EDM observed by SEM analysis (Figure 6a), and by the Raman spectra of the aged samples (Figure 7) which exibit some peaks at $\sim$ 278 cm^{-1}, $\sim$ 407 cm^{-1}, $\sim$ 478 cm^{-1}, $\sim$ 513 cm^{-1}, and $\sim$ 584 cm^{-1}, compatible with several forms of Mn dioxides and hydroxides according to [5].

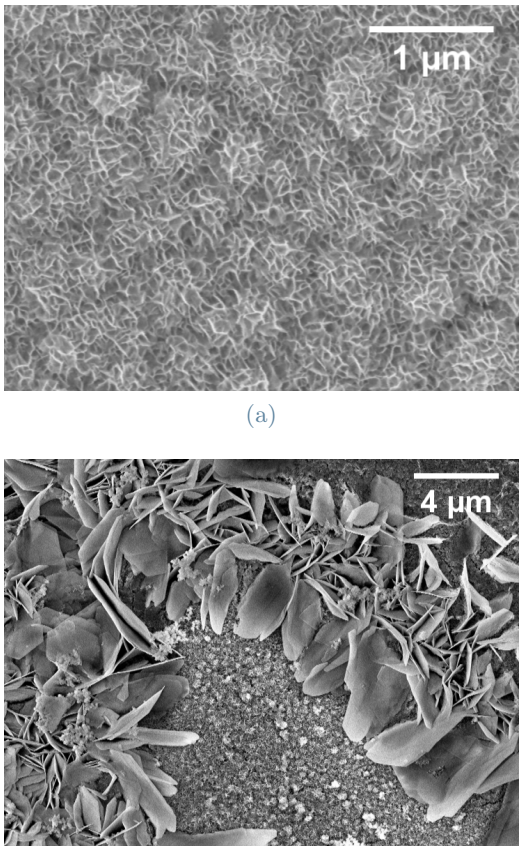

(a)

(b)

Figure 6: SEM images of the typical morphology of aged MnO_x samples in NS electrolyte (a) and in ZMS electrolyte (b).

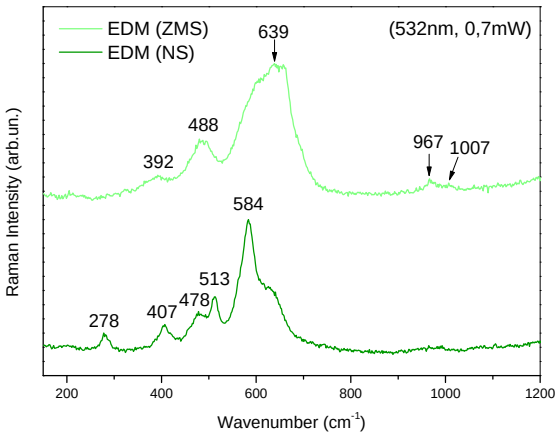

Figure 7: Raman spectra of EDM in NS (dark green) and ZMS (light green) electrolyte.

By normilising the 10th CV curve of each sample to the cathodic (negative current) minimum (Figure 8), I noticed that all the curves exhibit two anodic peaks (upper part of the graph), related to the progressive oxidation of Mn^{2+} to Mn^{3+} and Mn^{4+}, and two cathodic peaks (lower part of the graph) related to reduction of Mn^{3+} to Mn^{4+} and to Mn^{2+} dissolution. Moreover, as-deposited samples exhibit CV curves very different from each other and the effect of porosity is mainly visible in the anodic part of the curves. On the other hand annealed samples show much more similar curves but the effect of porosity is smaller. This similarity may be due to the same starting Mn_2O_3 phase, and to the sintering effect coming from the annealing treatment which contributes to homogenize the porosity differences. Lastly, I excluded any hypotesis of Na^{2+} ions intercalation due to the absence of any related feature at the beginning of the CV curves (around 0 V vs. Pt-QRef.).

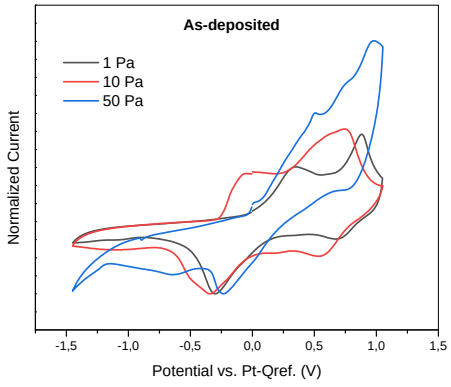

(a)

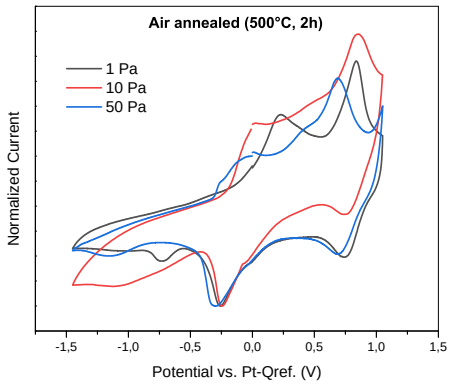

(b)

Figure 8: Normalized CVs (10th cycle) for as-deposited (a) and air annealed (500°C for 2 h) samples (b) in NS electrolyte.

Results regarding the samples annealed in vacuum are not reported since it was not possible to perform CV measurements due to their extremely low electronic conductivity.

On the other hand, CV measurements performed in the ZMS electrolyte were used to investigate the effect of Zn^{2+} ions on the electrochemical behaviour of MnO_x films. The CV parameters used are the same as for the case of NS electrolyte (scan rate of 10 mV/s, 10 cycles) except for the potential range which was reduced between -1 and 1.05 V in order to avoid the plating/stripping of Zn at very low cathodic potentials. The tests were performed only on three selected samples representative of all the phases: as-deposited Mn_3O_4 at 1 Pa, as deposited MnO_2 at 10 Pa, and Mn_2O_3 obtained after annealing in air (500°C, 2 h) of the sample deposited at 10 Pa.
In general, the presence of Zn^{2+} and Mn^{2+} ions in the electrolyte leads to a qualitative change of the shape of the curves both in the general behaviour and on the final result. This is confirmed also by SEM and Raman analysis which reveal the formation of zinc hydroxide sulfate (ZHS) recognisable by its flake-like morphology (Figure 6b) and by the rise of two small peaks at $\sim$ 967 cm^{-1} and $\sim$ 1007 cm^{-1} in the Raman spectra of aged samples (Figure 7). On the other hand, in the left part of the spectrum I notice a structured band, with peaks at $\sim$ 392 cm^{-1}, $\sim$ 488 cm^{-1} and $\sim$ 639 cm^{-1} difficult to be assigned to a specific phase but reasonably related to a mix of MnO_x maybe containing also Zn^{2+} and/or water molecules [5]. Both in the case of NS and ZMS electrolyte, the electrochemical process leads to the formation of EDM, even if the two phases are not identical in the two electrolytes.
Furthermore, I noticed that a strong "tail" at negative currents appears (around 0 V vs. Pt-QRef.) in the CV of the MnO_2 phase aged in ZMS electrolyte. This may be index of a possible intercalation of Zn^{2+} ions. The same feature is not present in the CVs of the other two samples (Mn_3O_4 and Mn_2O_3) maybe because their structures are less favorable to Zn^{2+} ions intercalation.
Also in this case the CVs were normalised to the cathodic minumum (Figure 9) but no particular

similarities can be observed except for a rapid rise at the beginning of the anodic part of the CVs (≈ 0.2 V vs. Pt-QRef.) highlighted also by Rossi et al. [4].

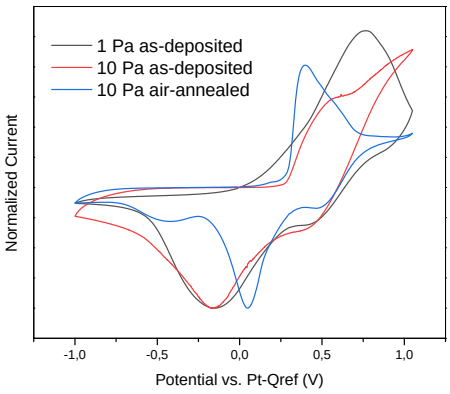

Figure 9: Normalised CVs (10^{th} cycle) of electrochemically aged samples in ZMS electrolyte.

The electrochemical investigation conducted in this thesis involved only preliminary experiments and a more detailed analysis should be carried out in order to draw comprehensive conclusions on the electrochemical behaviour of MnO_x materials.

6. Conclusions

In conclusion, the main objectives have been achieved and some interesting research insights arised. I was able to produce via PLD thin films of MnO_x and obtain different morphologies and phases by optimizing the deposition oxygen pressure and the temperature and atmosphere of the post-deposition annealing treatments. The extensive characterization of MnO_x films has revealed a variety of phases that can be obtained, and has contributed to better clarify their distinction. Finally, the first electrochemical tests, although they need to be extended, have been performed on thin films as model systems and they can be considered as a useful starting point for future electrochemical investigations of MnO_x in aqueous electrolyte.

References

[1] C. M. Julien and A. Mauger. Nanostructured MnO_2 as electrode materials for energy storage. *Nanomaterials*, 7(11):396, 2017.

[2] C. S. Casari and A. Li Bassi. Pulsed Laser Deposition of nanostructured oxides: From clusters to functional films. *Advances in Laser and Optics Research*, 7:65–100, 2011.

[3] Y. Xin, H. Cao, C. Liu, J. Chen, P. Liu, Y. Lu, and Z.C. Ling. A systematic spectroscopic study of laboratory synthesized manganese oxides relevant to mars. *J. Raman Spectroscopy*, 53:340–355, 2022.

[4] F. Rossi, E. Marini, M. Boniardi, A. Casaroli, A. Li Bassi, A. Macrelli, C. Mele, and B. Bozzini. What happens to MnO_2 when it comes in contact with Zn^{2+}? an electrochemical study in aid of Zn/MnO_2 -Based Rechargeable Batteries. *Energy Technol.*, 10(8):2200084, 2022.

[5] S. Bernardini, F. Bellatreccia, A. Casanova Municchia, G. Della Ventura, and A. Sodo. Raman spectra of natural manganese oxides. *J. Raman Spectroscopy*, 50:873–888, 2019.